

Soliton solutions for nonlocal Hirota equation with non-zero boundary conditions using Riemann-Hilbert method and PINN algorithm*

Wei-Qi Peng^a, Yong Chen^{a,b,*}

^a*School of Mathematical Sciences, Shanghai Key Laboratory of PMMP
East China Normal University, Shanghai, 200241, China*

^b*College of Mathematics and Systems Science, Shandong University
of Science and Technology, Qingdao, 266590, China*

Abstract

In this paper, we systematically investigate the nonlocal Hirota equation with nonzero boundary conditions via Riemann-Hilbert method and multi-layer physics-informed neural networks algorithm. Starting from the Lax pair of nonzero nonlocal Hirota equation, we first give out the Jost function and scattering matrix and their symmetry and asymptotic behavior. Then, the Riemann-Hilbert problem with nonzero boundary conditions are constructed and the precise formulae of N -soliton solution is written by determinants. Whereafter, the multi-layer physics-informed neural networks algorithm is applied to research the data-driven soliton solutions of the nonzero nonlocal Hirota equation by using the training data obtained from the Riemann-Hilbert method. Most strikingly, the integrable nonlocal equation is firstly solved via multi-layer physics-informed neural networks algorithm. As we all know, the nonlocal equations contain the \mathcal{PT} symmetry $\mathcal{P} : x \rightarrow -x$, or $\mathcal{T} : t \rightarrow -t$, which are different different with local ones. Adding the nonlocal term into the NN, we can successfully solve the integrable nonlocal Hirota equation by multi-layer physics-informed neural networks algorithm. The numerical results indicate the algorithm can well recover the data-driven soliton solutions of the integrable nonlocal equation. Noteworthily, the inverse problems of the integrable nonlocal equation are discussed for the first time through applying the physics-informed neural networks algorithm to discover the parameters of the equation in terms of its soliton solution.

Key words: Nonlocal Hirota equation; Riemann-Hilbert method; Nonzero boundary conditions; Soliton solutions; Physics-informed neural networks algorithm.

PACS numbers: 02.30.Ik, 05.45.Yv, 04.20.Jb.

*Corresponding authors.

E-mail addresses: ychen@sei.ecnu.edu.cn (Y. Chen)

1 Introduction

It is well-known that nonlinear partial differential equation (PDE) plays a prominent role in the subjects of mathematical physics, such as fluid mechanics, nonlinear optics, ocean communication, etc. In the history of soliton theory, finding exact solutions of integrable PDE is still a crucial issue. During the past several decades, in order to solve nonlinear evolution equations, more and more methods and techniques have been presented, including Hirota bilinear method [1], Darboux transformation (DT) [2], Inverse Scattering transformation (IST) [3], physics-informed neural networks (PINN) deep learning method [4], etc. Among them, IST method is one of the most powerful techniques to analyse the Cauchy problems of integrable nonlinear evolution equations. In 1967, Gardner et al. came up with this method first to handle the KdV equation with initial value problem [5]. However, for the classic IST method, it is not convenient to solve the Gel'fand-Levitan-Marchenko (GLM) integral equations. Therefore, Zakharov et al. simplifies the IST method by developing a Riemann-Hilbert (RH) formulation to replace the GLM equation [6]. After that, the RH formulation has been constantly applied to numerous integrable equations with zero boundary conditions (ZBCs), such as coupled nonlinear Schrödinger (NLS) equation, derivative Schrödinger equation, Sasa-Satsuma equation, and so on [7–14]. Recently, the RH method was also applied to construct the soliton solutions [15–19] and the rogue waves [20–22] for the integrable equations with nonzero boundary conditions (NZBCs).

With the rapid development of machine learning methods, deep learning has become a powerful tool for solving PDE. Recently, a new neural network (NN), named PINN, was recently proposed, which can be used to accomplish the high-dimensional network tasks with fewer data sets [4]. Besides, it is verified that PINN is very effective for solving and inverting equations controlled by mathematical physical systems. Later on, using PINN method to generate data-driven solutions and reveal the dynamic behavior of nonlinear partial differential equations with physical constraints has attracted extensive attention and raised a hot wave of research. Very recently, in terms of PINN method, Chen group constructed data-driven soliton solution, high-order breather wave, rogue wave, rogue periodic wave for several types of nonlinear evolution equations including KdV equation, NLS equation, KN equation, KP equation, Manakov system, etc. [23–28]. Particularly, based on conserved quantities, a two-stage PINN method is used to derive some data-driven localized wave solutions [29]. Besides, other scholars have also got some important results on data-driven solutions for the defocusing NLS equation with a potential, high-order NLS equation and coupled NLS equation [30–33].

The parity-time (\mathcal{PT}) symmetry, first proposed in quantum mechanics by Bender and his coworkers, plays an important role in characterizing the wave propagation for the NLS equation in mechanical systems, optical fibers and magnetism [34–36]. Up to now, the research of \mathcal{PT} system has made great progress in both theory and application [37–39]. For instance, Ablowitz and Musslimani first introduced the \mathcal{PT} symmetry to the well-known AKNS system by raising a nonlocal (also named reverse-space) NLS equation [40]

$$u_t(x, t) - iu_{xx}(x, t) \pm 2iQ(x, t)u(x, t) = 0, \quad Q(x, t) = u(x, t)u^*(-x, t), \quad (1.1)$$

which includes the \mathcal{PT} symmetric potential $Q(x, t)$ and satisfies the \mathcal{PT} symmetry restriction $Q(x, t) = Q^*(-x, t)$. The $*$ represents complex conjugate, and $Q(x, t)$ denotes electric

field envelope and complex refractive index distribution of beam. Since then, Fokas extended the nonlocal NLS equation to a higher dimensional form [41]. Moreover, other nonlocal integrable equations were also investigated, such as nonlocal Davey-Stewartson equations, nonlocal modified KdV equation, nonlocal sine-Gordon equation, nonlocal derivative NLS equation, etc. [42–48]. It's worth mentioning that several nonlocal integrable equations with NZBCs have been researched through developing the IST [49, 50]. After that, soliton solutions and high-order pole solutions for both focusing and defocusing nonlocal mKdV equations with NZBCs at infinity have been presented by a systematical inverse scattering transform [51, 52].

Recently, an integrable nonlocal (also named reverse-space-time) Hirota equation

$$q_t + \delta [q_{xx} - 2q^2 q^*(-x, -t)] + \beta [q_{xxx} - 6qq^*(-x, -t)q_x] = 0, \quad (1.2)$$

was constructed in Ref. [53]. Of which $\delta, \beta \in \mathbb{R}$ are arbitrary parameters. When $\delta = 1, \beta = 0$, Eq.(1.2) reduces to the reverse-space-time nonlocal NLS equation, and Eq.(1.2) changes into the reverse-space-time nonlocal complex mKdV equation at the case of $\delta = 0, \beta = 1$. Besides, for the \mathcal{PT} symmetric case $q^*(-x, -t) = q(x, t)$, Eq.(1.2) becomes the usual Hirota equation. The explicit multi-soliton solutions were generated for Eq.(1.2) by employing Hirota's direct method as well as Darboux-Crum transformations [53]. In what follows, we would like to analyse its Lax pair firstly based on the early results [53].

We started the analysis with the AKNS program

$$\begin{aligned} \Psi_x &= U\Psi, & U &\equiv \begin{pmatrix} -i\lambda & q(x, t) \\ r(x, t) & i\lambda \end{pmatrix}, \\ \Psi_t &= V\Psi, & V &\equiv \begin{pmatrix} A(x, t) & B(x, t) \\ C(x, t) & -A(x, t) \end{pmatrix}, \\ A &= \delta qr + 2\delta\lambda^2 + \beta(rq_x - qr_x - 4i\lambda^3 - 2i\lambda qr), \\ B &= -\delta q_x + 2i\delta\lambda q + \beta(2q^2 r - q_{xx} + 2i\lambda q_x + 4\lambda^2 q), \\ C &= \delta r_x + 2i\delta\lambda r + \beta(2qr^2 - r_{xx} - 2i\lambda r_x + 4\lambda^2 r), \end{aligned} \quad (1.3)$$

where $\Psi = \Psi(x, t, \lambda)$ on behalf of the eigenfunction, and λ is the spectral parameter. $q(x, t)$ and $r(x, t)$ are the potential function. According to the compatibility conditions of above system (1.3), i. e. $U_t - V_x + [U, V] = 0$, we obtain

$$\begin{aligned} q_t + \delta [q_{xx} - 2q^2 r] + \beta [q_{xxx} - 6qrq_x] &= 0, \\ r_t - \delta [r_{xx} - 2qr^2] + \beta [r_{xxx} - 6qrr_x] &= 0. \end{aligned} \quad (1.4)$$

By the symmetry reduction

$$r(x, t) = q^*(-x, -t), \quad (1.5)$$

the nonlocal Hirota equation (1.2) can be derived. Hence, the Eq.(1.2) meets following

Lax pairs

$$\begin{aligned}
\Psi_x &= U\Psi, & U &\equiv \begin{pmatrix} -i\lambda & q(x,t) \\ q^*(-x,-t) & i\lambda \end{pmatrix}, \\
\Psi_t &= V\Psi, & V &\equiv \begin{pmatrix} \tilde{A}(x,t) & \tilde{B}(x,t) \\ \tilde{C}(x,t) & -\tilde{A}(x,t) \end{pmatrix}, \\
\tilde{A} &= \delta q q^*(-x,-t) + 2\delta\lambda^2 + \beta [q^*(-x,-t)q_x - q q_x^*(-x,-t) - 4i\lambda^3 - 2i\lambda q q^*(-x,-t)], \\
\tilde{B} &= -\delta q_x + 2i\delta\lambda q + \beta [2q^2 q^*(-x,-t) - q_{xx} + 2i\lambda q_x + 4\lambda^2 q], \\
\tilde{C} &= \delta q_x^*(-x,-t) + 2i\delta\lambda q^*(-x,-t) \\
&+ \beta [2q q^*(-x,-t)^2 - q_{xx}^*(-x,-t) - 2i\lambda q_x^*(-x,-t) + 4\lambda^2 q^*(-x,-t)]. \tag{1.6}
\end{aligned}$$

To the best of our knowledge, although some people have studied the nonlocal Hirota equation with ZBCs [54–56], the studies of the nonlocal Hirota Eq.(1.2) with NZBCs have been rarely reported via using RH method, as well as the RH method with NZBCs is more complicated than one with ZBCs. In what follows, we would systematically consider the matrix RH problem for the nonlocal Hirota Eq.(1.2) with following NZBCs at infinity

$$\lim_{x \rightarrow \pm\infty} q(x,t) = q_{\pm} e^{2\delta q_0^2 t}, \tag{1.7}$$

where $|q_{\pm}| = q_0 > 0$, and $q_+ = q_-$ are constant. Different from previous work about the usual Hirota equation, the nonlocal Hirota equation involves different symmetry reductions and disparate discrete spectra distribution. Furthermore, we also find that PINN deep learning for solving nonlocal integrable equation has not been researched so far. Therefore, in this paper, we also commit to propose a scheme to solve integrable nonlocal equation in terms of PINN method. As an example, we choose the integrable nonzero nonlocal Hirota equation to highlight the ability of our strategy to handle the integrable nonlocal equation, and successfully predict the data-driven soliton solution of the nonzero nonlocal Hirota equation. On the other hand, we also discuss the data-driven parameter discovery for the nonzero nonlocal Hirota equation.

The outline of this paper is organized as follows: In section 2, we carry out the spectral analysis for nonlocal Hirota equation under NZBCs, and derive the corresponding Lax pair, Jost solutions, scattering matrix and their symmetry reductions. In section 3, through analysing the inverse scattering problem for nonlocal Hirota equation under NZBCs, we establish the RH problem for the nonlocal Hirota equation under NZBCs and obtain the explicit N -soliton solutions for the reflectionless coefficients under NZBCs. In section 4, the data-driven soliton solutions and data-driven parameter discovery for the nonlocal Hirota equation are researched via PINN method. Finally, some summaries are given in the last section.

2 Spectral analysis for nonlocal Hirota equation under NZBCs

2.1 Lax pair and Jost solutions

In order to facilitate the later calculation, we deal with Lax pair (1.6) with the boundary condition (1.7) at the beginning. Let's make an appropriate transformation

$$q \rightarrow qe^{2\delta q_0^2 t}, \quad \Psi \rightarrow e^{\delta q_0^2 t \sigma_3} \Psi, \quad (2.1)$$

where σ_3 is one of the following Pauli matrices

$$\sigma_1 = \begin{pmatrix} 0 & 1 \\ 1 & 0 \end{pmatrix}, \quad \sigma_2 = \begin{pmatrix} 0 & -i \\ i & 0 \end{pmatrix}, \quad \sigma_3 = \begin{pmatrix} 1 & 0 \\ 0 & -1 \end{pmatrix}. \quad (2.2)$$

Then, the nonlocal Hirota equation (1.2) changes into

$$q_t + \delta [q_{xx} - 2q^2 q^*(-x, -t) + 2q_0^2 q] + \beta [q_{xxx} - 6qq^*(-x, -t)q_x] = 0, \quad (2.3)$$

with following boundary

$$\lim_{x \rightarrow \pm\infty} q(x, t) = q_{\pm}, \quad (2.4)$$

which admits the Lax pair

$$\begin{aligned} \Psi_x = U\Psi, \quad U &\equiv \begin{pmatrix} -i\lambda & q(x, t) \\ q^*(-x, -t) & i\lambda \end{pmatrix}, \\ \Psi_t = V\Psi, \quad V &\equiv \begin{pmatrix} \tilde{A}(x, t) - \delta q_0^2 & \tilde{B}(x, t) \\ \tilde{C}(x, t) & -\tilde{A}(x, t) + \delta q_0^2 \end{pmatrix}. \end{aligned} \quad (2.5)$$

As $x \rightarrow \pm\infty$, the Lax pair (2.5) under the boundary (2.4) becomes

$$\Psi_x = U_{\pm}\Psi = (-i\lambda\sigma_3 + Q_{\pm})\Psi, \quad \Psi_t = V_{\pm}\Psi = [2i\delta\lambda + \beta(4\lambda^2 + 2q_0^2)] U_{\pm}\Psi, \quad (2.6)$$

where

$$Q_{\pm} = \begin{pmatrix} 0 & q_{\pm} \\ q_{\mp}^* & 0 \end{pmatrix}. \quad (2.7)$$

The system (2.6) can be solved by

$$\Psi_{\pm}^{bg}(x, t, \lambda) = \begin{cases} Y_{\pm}(\lambda)e^{-i\theta(x, t, \lambda)\sigma_3}, & \lambda \neq \pm q_0 \\ I + (x + (2i\delta\lambda + \beta(4\lambda^2 + 2q_0^2))t) U_{\pm}(\lambda), & \lambda = \pm q_0, \end{cases} \quad (2.8)$$

where

$$Y_{\pm} = \begin{pmatrix} 1 & -\frac{iq_{\pm}}{\lambda+k} \\ \frac{iq_{\pm}^*}{\lambda+k} & 1 \end{pmatrix}, \quad \theta(x, t, k) = k[x + (2i\delta\lambda + \beta(4\lambda^2 + 2q_0^2))t], \quad k^2 = \lambda^2 - q_0^2. \quad (2.9)$$

In order to analyse the scattering problem on a standard z -plane instead of the two-sheeted Riemann surface, we introduce a uniformization variable $z = k + \lambda$, given by

$$k = \frac{1}{2}\left(z - \frac{q_0^2}{z}\right), \quad \lambda = \frac{1}{2}\left(z + \frac{q_0^2}{z}\right). \quad (2.10)$$

Setting D_+ , D_- and Σ on z -plane as $D_{\pm} = \{z \in \mathbb{C} | \text{Im}z \gtrless 0\}$, $\Sigma = \mathbb{R}$, the Jost solutions $\Psi_{\pm}(x, t, z)$ are defined by

$$\Psi_{\pm}(x, t, z) = Y_{\pm} e^{-i\theta(x, t, z)\sigma_3} + o(1), \quad z \in \Sigma, \quad \text{as } x \rightarrow \pm\infty. \quad (2.11)$$

Using the variable transformation

$$\mu_{\pm}(x, t, z) = \Psi_{\pm}(x, t, z) e^{i\theta(x, t, z)\sigma_3}, \quad (2.12)$$

we get the modified Jost solutions $\mu_{\pm}(x, t, z) \rightarrow Y_{\pm}(z)$ as $x \rightarrow \pm\infty$, which satisfies the following Volterra integral equations

$$\mu_{\pm}(x, t, z) = \begin{cases} Y_{\pm} + \int_{\pm\infty}^x Y_{\pm} e^{-ik(x-y)\hat{\sigma}_3} [Y_{\pm}^{-1} \Delta U_{\pm}(y, t) \mu_{\pm}(y, t, z)] dy, & z \neq \pm q_0, \\ Y_{\pm} + \int_{\pm\infty}^x [I + (x-y)U_{\pm}(z)] \Delta U_{\pm}(y, t) \mu_{\pm}(y, t, z) dy, & z = \pm q_0, \end{cases} \quad (2.13)$$

where $\Delta U_{\pm} = U - U_{\pm}$.

Proposition 2.1. *Assume $q - q_{\pm} \in L^1(\mathbb{R}^{\pm})$, then $\mu_{\pm}(x, t, z)$ defined in Eq.(2.12) uniquely solve the Volterra integral equation (2.13) in $\Sigma_0 = \Sigma \setminus \{\pm q_0\}$, and $\mu_{\pm}(x, t, z)$ yield:*

- $\mu_{-1}(x, t, z)$ and $\mu_{+2}(x, t, z)$ is analytical in D_+ and continuous in $D_+ \cup \Sigma_0$,
- $\mu_{+1}(x, t, z)$ and $\mu_{-2}(x, t, z)$ is analytical in D_- and continuous in $D_- \cup \Sigma_0$,
- $\mu_{\pm}(x, t, z) \rightarrow I$ as $z \rightarrow \infty$,
- $\mu_{\pm}(x, t, z) \rightarrow -\frac{i}{z}\sigma_3 Q_{\pm}$ as $z \rightarrow 0$,
- $\det \mu_{\pm}(x, t, z) = \det Y_{\pm} = \gamma = 1 - \frac{q_0^2}{z^2}$, $x, t \in \mathbb{R}$, $z \in \Sigma_0$.

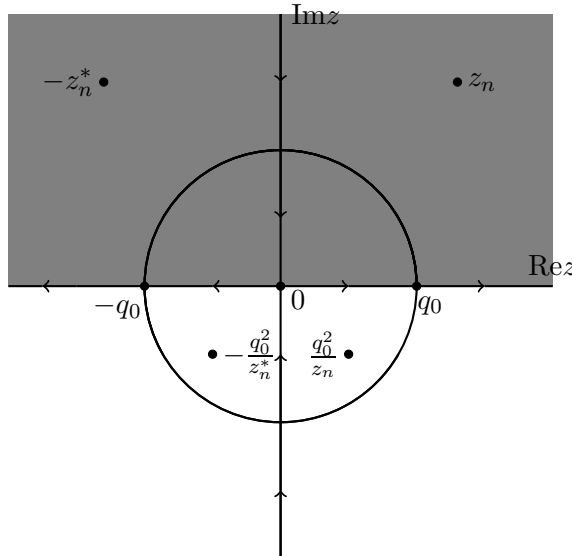


Figure 1. (Color online) Distribution of the discrete spectrum and jumping curves for the RH problem on complex z -plane, Region $D_+ = \{z \in \mathbb{C} | \text{Im}z > 0\}$ (gray region), region $D_- = \{z \in \mathbb{C} | \text{Im}z < 0\}$ (white region).

Since the Jost solutions $\Psi_{\pm}(x, t, z)$ are the simultaneous solutions of Lax pair (2.5), we can establish the linear relation by a scattering matrix $S(z) = (s_{ij}(z))_{2 \times 2}$, given by

$$\Psi_+(x, t, z) = \Psi_-(x, t, z)S(z), \quad z \in \Sigma_0. \quad (2.14)$$

We can write the scattering coefficients into the form of Wronskians determinant

$$\begin{aligned} s_{11}(z) &= \frac{Wr(\Psi_{+,1}, \Psi_{-,2})}{\gamma(z)}, & s_{12}(z) &= \frac{Wr(\Psi_{+,2}, \Psi_{-,2})}{\gamma(z)}, \\ s_{21}(z) &= \frac{Wr(\Psi_{-,1}, \Psi_{+,1})}{\gamma(z)}, & s_{22}(z) &= \frac{Wr(\Psi_{-,1}, \Psi_{+,2})}{\gamma(z)}. \end{aligned} \quad (2.15)$$

Proposition 2.2. *Suppose $q - q_{\pm} \in L^1(\mathbb{R}^{\pm})$, then the scattering matrix $S(z)$ has the following characteristics:*

- $\det S(z) = 1$ for $z \in \Sigma_0$,
- $s_{22}(z)$ is analytical in D_+ and continuous in $D_+ \cup \Sigma_0$,
- $s_{11}(z)$ is analytical in D_- and continuous in $D_- \cup \Sigma_0$,
- $S(x, t, z) \rightarrow I$ as $z \rightarrow \infty$,
- $S(x, t, z) \rightarrow I$ as $z \rightarrow 0$.

2.2 Symmetry reductions

In this subsection, according to the reduction conditions of the Lax pair on the complex z -plane, the symmetries of the Jost solutions $\Psi(x, t, z)$ and scattering matrix $S(z)$ are studied for the nonlocal Hirota equation with NZBCs. The details are as follows:

Proposition 2.3. *The $X(x, t, z)$ and $T(x, t, z)$ in the Lax pair (2.5) meet the following reduction conditions on z -plane:*

- *The first symmetry reduction*

$$U(x, t, z) = -\sigma_2 U(-x, -t, -z^*)^* \sigma_2, \quad V(x, t, z) = -\sigma_2 V(-x, -t, -z^*)^* \sigma_2. \quad (2.16)$$

- *The second symmetry reduction*

$$U(x, t, z) = U(x, t, \frac{q_0^2}{z}), \quad V(x, t, z) = V(x, t, \frac{q_0^2}{z}). \quad (2.17)$$

Proposition 2.4. *The Jost solutions $\Psi(x, t, z)$ and scattering matrix $S(z)$ possess the following reduction conditions on z -plane:*

- *The first symmetry reduction*

$$\Psi_{\pm}(x, t, z) = \sigma_2 \Psi_{\mp}(-x, -t, -z^*)^* \sigma_2, \quad S(z) = \sigma_2 S^*(-z^*)^{-1} \sigma_2. \quad (2.18)$$

- *The second symmetry reduction*

$$\Psi_{\pm}(x, t, z) = -\frac{i}{z} \Psi_{\pm}(x, t, \frac{q_0^2}{z}) \sigma_3 Q_{\pm}, \quad S(z) = Q_-^{-1} \sigma_3 S(\frac{q_0^2}{z}) \sigma_3 Q_+. \quad (2.19)$$

2.3 Discrete spectrum with simple poles

In this subsection, assuming that $s_{22}(z)$ has N simple zeros z_n ($n = 1, 2, \dots, N$) in $D_+ \cap \{z \in \mathbb{C} : \text{Re} z > 0\}$, then we have $s_{22}(z_0) = 0$ and $s'_{22}(z_0) \neq 0$ in the situations of z_0 being the simple zero of $s_{22}(z)$. In terms of the symmetries of the scattering matrix, the corresponding discrete spectrum is summarized into (see Fig. 1)

$$\Upsilon = \left\{ z_n, -z_n^*, \frac{q_0^2}{z_n}, -\frac{q_0^2}{z_n^*} \right\}_{n=1}^N. \quad (2.20)$$

Considering $s_{22}(z_0) = 0$ ($z_0 \in \Upsilon \cap D_+$), it is not hard to find that $\Psi_{-1}(x, t, z_0)$ and $\Psi_{+2}(x, t, z_0)$ are linearly dependent. Homoplastically, $\Psi_{+1}(x, t, z_0)$ and $\Psi_{-2}(x, t, z_0)$ are linearly dependent because of $s_{11}(z_0) = 0$ ($z_0 \in \Upsilon \cap D_-$). Then, one has

$$\begin{aligned} \Psi_{+2}(x, t, z_0) &= b[z_0] \Psi_{-1}(x, t, z_0), & z_0 \in \Upsilon \cap D_+, \\ \Psi_{+1}(x, t, z_0) &= b[z_0] \Psi_{-2}(x, t, z_0), & z_0 \in \Upsilon \cap D_-, \end{aligned} \quad (2.21)$$

where $b[z_0]$ is a undetermined parameter. Therefore, we arrive at

$$\begin{aligned} \text{Res}_{z=z_0} \left[\frac{\Psi_{+2}(x, t; z)}{s_{22}(z)} \right] &= A[z_0] \Psi_{-1}(x, t; z_0), & z_0 \in \Upsilon \cap D_+, \\ \text{Res}_{z=z_0} \left[\frac{\Psi_{+1}(x, t; z)}{s_{11}(z)} \right] &= A[z_0] \Psi_{-2}(x, t; z_0), & z_0 \in \Upsilon \cap D_-, \end{aligned} \quad (2.22)$$

where

$$A[z_0] = \begin{cases} \frac{b[z_0]}{s'_{22}(z_0)}, & z_0 \in \Upsilon \cap D_+ \\ \frac{b[z_0]}{s'_{11}(z_0)}, & z_0 \in \Upsilon \cap D_- \end{cases} \quad (2.23)$$

Proposition 2.5. *Two relations for $b[z_0]$, $s'_{22}(z_0)$ and $s'_{11}(z_0)$ are got below:*

- *The first relation*

$$b[z_0] = -\frac{1}{b[-z_0^*]^*}, \quad s'_{11}(z_0) = -s'_{11}(-z_0^*)^*, \quad s'_{22}(z_0) = -s'_{22}(-z_0^*)^*. \quad (2.24)$$

- *The second relation*

$$\begin{aligned} b[z_0] &= -\frac{q_+}{q_-^*} b\left[\frac{q_0^2}{z_0}\right], & s'_{22}(z_0) &= -\frac{q_0^2}{z_0^2} s'_{11}\left(\frac{q_0^2}{z_0}\right), & z_0 \in D_+, \\ b[z_0] &= -\frac{q_+^*}{q_-} b\left[\frac{q_0^2}{z_0}\right], & s'_{11}(z_0) &= -\frac{q_0^2}{z_0^2} s'_{22}\left(\frac{q_0^2}{z_0}\right), & z_0 \in D_-. \end{aligned} \quad (2.25)$$

3 Inverse scattering problem for nonlocal Hirota equation under NZBCs

3.1 The Riemann-Hilbert problem under NZBCs

In terms of the analyticity of Jost solutions $\mu_{\pm}(x, t, z)$ in Proposition 2.1, the following sectionally meromorphic matrices can be defined

$$M_{-}(x, t, z) = \left(\frac{\mu_{+1}}{s_{11}}, \mu_{-2} \right), \quad M_{+}(x, t, z) = \left(\mu_{-1}, \frac{\mu_{+2}}{s_{22}} \right), \quad (3.1)$$

where \pm represent analyticity in D_{+} and D_{-} , respectively. Subsequently, a matrix RH problem is constructed:

Riemann-Hilbert Problem $M(x, t, z)$ solves the following RHP:

$$\begin{cases} M(x, t, z) \text{ is analytic in } \mathbb{C} \setminus \Sigma, \\ M_{-}(x, t, z) = M_{+}(x, t, z)(I - G(x, t, z)), & z \in \Sigma, \\ M(x, t, z) \rightarrow I, & z \rightarrow \infty, \\ M(x, t, z) \rightarrow -\frac{i}{z}\sigma_3 Q_{-}, & z \rightarrow 0, \end{cases} \quad (3.2)$$

of which the jump matrix $G(x, t, z)$ is

$$G = \begin{pmatrix} \rho(z)\tilde{\rho}(z) & e^{-2i\theta(x,t,z)}\tilde{\rho}(z) \\ -e^{2i\theta(x,t,z)}\rho(z) & 0 \end{pmatrix}, \quad (3.3)$$

where $\rho(z) = \frac{s_{21}(z)}{s_{11}(z)}$, $\tilde{\rho}(z) = \frac{s_{12}(z)}{s_{22}(z)}$. Let

$$M(x, t, z) = I + \frac{1}{z}M^{(1)}(x, t; z) + O\left(\frac{1}{z^2}\right), \quad z \rightarrow \infty, \quad (3.4)$$

then the potential $q(x, t)$ of the nonlocal Hirota equation (1.2) with NZBCs is given by

$$q(x, t) = iM_{12}^{(1)}(x, t, z) = i \lim_{z \rightarrow \infty} zM_{12}(x, t, z). \quad (3.5)$$

As a matter of convenience, we take $\hat{\zeta}_n = \frac{q_n^2}{\zeta_n}$ and define

$$\zeta_n = \begin{cases} z_n, & n = 1, 2, \dots, N \\ -z_{n-N}^*, & n = N+1, N+2, \dots, 2N \end{cases} \quad (3.6)$$

Then the residue of $M(x, t, z)$ is

$$\begin{aligned} \operatorname{Res}_{z=\zeta_n} M_{+} &= \left(0, A[\zeta_n]e^{-2i\theta(x,t,\zeta_n)}\mu_{-1}(x, t, \zeta_n) \right), \\ \operatorname{Res}_{z=\hat{\zeta}_n} M_{-} &= \left(A[\hat{\zeta}_n]e^{2i\theta(x,t,\hat{\zeta}_n)}\mu_{-2}(x, t, \hat{\zeta}_n), 0 \right). \end{aligned} \quad (3.7)$$

through subtracting out the residue and the asymptotic values as $z \rightarrow \infty, z \rightarrow 0$ from the original non-regular RHP, the following regular RHP can be obtained

$$\begin{aligned} M_{-} + \frac{i}{z}\sigma_3 Q_{-} - I - \sum_{n=1}^{2N} \left[\frac{\operatorname{Res}_{z=\zeta_n} M_{+}}{z - \zeta_n} + \frac{\operatorname{Res}_{z=\hat{\zeta}_n} M_{-}}{z - \hat{\zeta}_n} \right] = \\ M_{+} + \frac{i}{z}\sigma_3 Q_{-} - I - \sum_{n=1}^{2N} \left[\frac{\operatorname{Res}_{z=\zeta_n} M_{+}}{z - \zeta_n} + \frac{\operatorname{Res}_{z=\hat{\zeta}_n} M_{-}}{z - \hat{\zeta}_n} \right] - M_{+} G. \end{aligned} \quad (3.8)$$

which can be solved by the Plemelj's formulae, given by

$$M(x, t; z) = I - \frac{i}{z} \sigma_3 Q_- + \frac{1}{2\pi i} \int_{\Sigma} \frac{M_+(x, t; \zeta) G(x, t; \zeta)}{\zeta - z} d\zeta + \sum_{n=1}^{2N} \left[\frac{\text{Res}_{z=\zeta_n} M_+}{z - \zeta_n} + \frac{\text{Res}_{z=\hat{\zeta}_n} M_-}{z - \hat{\zeta}_n} \right]. \quad (3.9)$$

where

$$\frac{\text{Res}_{z=\zeta_n} M_+}{z - \zeta_n} + \frac{\text{Res}_{z=\hat{\zeta}_n} M_-}{z - \hat{\zeta}_n} = \left(\hat{C}_n(z) \mu_{-2}(\hat{\zeta}_n), C_n(z) \mu_{-1}(\zeta_n) \right), \quad (3.10)$$

and

$$C_n(z) = \frac{A[\zeta_n] e^{-2i\theta(\zeta_n)}}{z - \zeta_n}, \quad \hat{C}_n(z) = \frac{A[\hat{\zeta}_n] e^{2i\theta(\hat{\zeta}_n)}}{z - \hat{\zeta}_n}. \quad (3.11)$$

Furthermore, according to (3.4), one has

$$M^{(1)}(x, t, z) = -\frac{1}{2\pi i} \int_{\Sigma} M_+(x, t; \zeta) G(x, t; \zeta) d\zeta - i\sigma_3 Q_- + \sum_{n=1}^{2N} \left(A[\hat{\zeta}_n] e^{2i\theta(\hat{\zeta}_n)} \mu_{-2}(\hat{\zeta}_n), A[\zeta_n] e^{-2i\theta(\zeta_n)} \mu_{-1}(\zeta_n) \right). \quad (3.12)$$

Therefore, the potential $q(x, t)$ with simple poles for the nonlocal Hirota equation with NZBCs is given by

$$q(x, t) = iM_{12}^{(1)} = q_- + i \sum_{n=1}^{2N} A[\zeta_n] e^{-2i\theta(\zeta_n)} \mu_{-11}(\zeta_n) - \frac{1}{2\pi} \int_{\Sigma} (M_+(x, t; \zeta) G(x, t; \zeta))_{12} d\zeta. \quad (3.13)$$

3.2 Trace formulae and theta condition

The scattering coefficients $s_{22}(z)$ and $s_{11}(z)$ respectively have simple zeros ζ_n and $\hat{\zeta}_n$, thus we can take

$$\beta^+(z) = s_{22}(z) \prod_{n=1}^{2N} \frac{z - \hat{\zeta}_n}{z - \zeta_n}, \quad \beta^-(z) = s_{11}(z) \prod_{n=1}^{2N} \frac{z - \zeta_n}{z - \hat{\zeta}_n}, \quad (3.14)$$

that means $\beta^+(z)$ is analytic and has no zeros in D_+ , and $\beta^-(z)$ is analytic and has no zeros in D_- . Also, $\beta^{\pm}(z) \rightarrow o(1)$ as $z \rightarrow \infty$. According to the Plemelj's formulae, $\beta^{\pm}(z)$ can be written as

$$\log \beta^{\pm}(z) = \mp \frac{1}{2\pi i} \int_{\Sigma} \frac{\log(1 - \rho \tilde{\rho})}{s - z} ds, \quad z \in D^{\pm}. \quad (3.15)$$

Using Eq.(3.14), we derive the following trace formulae

$$\begin{aligned} s_{22}(z) &= \exp \left[-\frac{1}{2\pi i} \int_{\Sigma} \frac{\log(1 - \rho\tilde{\rho})}{s - z} ds \right] \prod_{n=1}^{2N} \frac{z - \zeta_n}{z - \hat{\zeta}_n}, \\ s_{11}(z) &= \exp \left[\frac{1}{2\pi i} \int_{\Sigma} \frac{\log(1 - \rho\tilde{\rho})}{s - z} ds \right] \prod_{n=1}^{2N} \frac{z - \hat{\zeta}_n}{z - \zeta_n}. \end{aligned} \quad (3.16)$$

Let $z \rightarrow 0$ in the first formula of Eq.(3.16), one has

$$\exp \left[\frac{i}{2\pi} \int_{\Sigma} \frac{\log(1 - \rho\tilde{\rho})}{s} ds \right] \prod_{n=1}^N \frac{|z_n|^4}{q_0^4} = 1. \quad (3.17)$$

In addition, taking the derivative of the Eq.(3.16) with respect to z , we obtain $s'_{22}(\zeta_j)$ and $s'_{11}(\hat{\zeta}_j)$, given by

$$\begin{aligned} s'_{22}(\zeta_j) &= \exp \left[-\frac{1}{2\pi i} \int_{\Sigma} \frac{\log(1 - \rho\tilde{\rho})}{s - \zeta_j} ds \right] \frac{\prod_{m \neq j} (\zeta_j - \zeta_m)}{\prod_{m=1}^{2N} (\zeta_j - \hat{\zeta}_m)}, \\ s'_{11}(\hat{\zeta}_j) &= \exp \left[\frac{1}{2\pi i} \int_{\Sigma} \frac{\log(1 - \rho\tilde{\rho})}{s - \hat{\zeta}_j} ds \right] \frac{\prod_{m \neq j} (\hat{\zeta}_j - \zeta_m)}{\prod_{m=1}^{2N} (\hat{\zeta}_j - \zeta_m)}. \end{aligned} \quad (3.18)$$

3.3 The solution of nonlocal Hirota equation under NZBCs

In the case of no reflection, i. e. $\rho(z) = \tilde{\rho}(z) = 0$, we can get the soliton solution. We first take the second column of Eq.(3.9)

$$\mu_{-2}(z) = \begin{pmatrix} -\frac{i}{z}q_- \\ 1 \end{pmatrix} + \sum_{n=1}^{2N} C_n(z)\mu_{-1}(\zeta_n). \quad (3.19)$$

In terms of the symmetric relation, we easily get

$$\mu_{-2}(z) = -\frac{iq_-}{z}\mu_{-1}\left(\frac{q_0^2}{z}\right). \quad (3.20)$$

Substituting Eq.(3.20) into Eq. (3.19), and setting $z = \hat{\zeta}_j, j = 1, 2, \dots, 2N$, we generate a $2N$ linear system:

$$\sum_{n=1}^{2N} \left(C_n(\hat{\zeta}_j) + \frac{iq_-}{\hat{\zeta}_j} \delta_{j,n} \right) \mu_{-1}(\zeta_n) + \begin{pmatrix} -\frac{i}{\hat{\zeta}_j}u_- \\ 1 \end{pmatrix} = 0. \quad (3.21)$$

Theorem 3.1 *The precise formulae of N -soliton solution for the nonlocal Hirota equation (2.3) with NZBCs (2.4) is expressed as*

$$q(x, t) = q_- - i \frac{\det \begin{pmatrix} \mathcal{H} & \varphi \\ \chi^T & 0 \end{pmatrix}}{\det(\mathcal{H})}. \quad (3.22)$$

Proof. From Eq.(3.21), it is not hard to derive a $2N$ linear system with respect to $\mu_{-11}(\zeta_n)$

$$\sum_{n=1}^{2N} \left(C_n(\hat{\zeta}_j) + \frac{iq_-}{\hat{\zeta}_j} \delta_{j,n} \right) \mu_{-11}(\zeta_n) = \frac{iq_-}{\hat{\zeta}_j}, \quad j = 1, 2, \dots, 2N. \quad (3.23)$$

The linear system can be rewritten into a matrix form:

$$\mathcal{H}\alpha = \varphi, \quad (3.24)$$

where $\mathcal{H} = (h_{jn})_{2N \times 2N}$, $\alpha = (\alpha_n)_{2N \times 1}$, $\varphi = (\varphi_j)_{2N \times 1}$ with

$$h_{jn} = C_n(\hat{\zeta}_j) + \frac{iq_-}{\hat{\zeta}_j} \delta_{j,n}, \quad \alpha_n = \mu_{-11}(\zeta_n), \quad \varphi_j = \frac{iq_-}{\hat{\zeta}_j}. \quad (3.25)$$

In the case of reflectionless potential, Eq.(3.13) is rewritten as

$$q = q_- + i\chi^T \alpha, \quad (3.26)$$

where $\chi = (\chi_n)_{2N \times 1}$ with $\chi_n = A[\zeta_n]e^{-2i\theta(\zeta_n)}$. Combining Eq. (3.24), the expression of the soliton solution is presented finally. \square

As a example, through choosing some appropriate parameters, we discuss the dynamical behaviors for simple poles solution in the case of $N = 1$ and $N = 2$, respectively. It is worth mentioning that the discrete spectrum can not to be pure imaginary number, which is verified from Proposition 2.5.

Case 1: $N = 1$

Let $z_1 = q_0 e^{i\vartheta_1}$, $\vartheta_1 \in (0, \frac{\pi}{2})$. Then, from (3.6), we have $\zeta_1 = q_0 e^{i\vartheta_1}$, $\zeta_2 = -q_0 e^{-i\vartheta_1}$, $\hat{\zeta}_1 = q_0 e^{-i\vartheta_1}$, $\hat{\zeta}_2 = -q_0 e^{i\vartheta_1}$. Let $q_- = q_0 e^{i\theta_-}$, $\theta_- \in \{0, \pi\}$, $b[\zeta_1] = b_1$, where b_1 are all arbitrary parameter. From Proposition 2.5, we have $b[\zeta_2] = -\frac{1}{b_1^*}$. From Eq.(3.18), one has

$$\begin{aligned} s'_{22}(\zeta_1) &= \frac{\zeta_1 - \zeta_2}{(\zeta_1 - \hat{\zeta}_1)(\zeta_1 - \hat{\zeta}_2)} = \frac{\cos(\vartheta_1)}{2q_0 i e^{i\vartheta_1} \sin(\vartheta_1)}, \\ s'_{22}(\zeta_2) &= \frac{\zeta_2 - \zeta_1}{(\zeta_2 - \hat{\zeta}_1)(\zeta_2 - \hat{\zeta}_2)} = \frac{\cos(\vartheta_1)}{2q_0 i e^{-i\vartheta_1} \sin(\vartheta_1)}, \end{aligned} \quad (3.27)$$

then we have

$$A[\zeta_1] = \frac{b[\zeta_1]}{s'_{22}(\zeta_1)} = \frac{2q_0 b_1 i e^{i\vartheta_1} \sin(\vartheta_1)}{\cos(\vartheta_1)}, \quad A[\zeta_2] = \frac{b[\zeta_2]}{s'_{22}(\zeta_2)} = -\frac{2q_0 i e^{-i\vartheta_1} \sin(\vartheta_1)}{b_1^* \cos(\vartheta_1)}. \quad (3.28)$$

Thus the 1-eigenvalue solution of the nonlocal Hirota equation (2.3) is deduced as

$$q(x, t) = q_0 \frac{\Omega_1}{\Omega_2}, \quad (3.29)$$

where

$$\begin{aligned}
\Omega_1 &= (2 \sin(\vartheta_1) + i) \cos(\vartheta_1) \Theta_1 - (2 \sin(\vartheta_1) - i) b_1 b_1^* \cos(\vartheta_1) \Theta_2 + b_1^* \cos(\vartheta_1)^2 e^{3i\theta_-} \\
&\quad + 2ib_1 \sin(\vartheta_1) \Theta_3 (e^{-i\vartheta_1+i\theta_-} - e^{i\vartheta_1+i\theta_-}) + (3b_1 \cos(\vartheta_1)^2 - 4b_1) \Theta_3 e^{i\theta_-} \\
\Omega_2 &= i \cos(\vartheta_1) \Theta_1 e^{i\vartheta_1-i\theta_-} + ib_1 b_1^* \cos(\vartheta_1) \Theta_2 e^{-i\vartheta_1-i\theta_-} - b_1 \Theta_3 \\
&\quad + (1 - \cos(\vartheta_1)^2) b_1 \Theta_4 + b_1^* \cos(\vartheta_1)^2 e^{2i\theta_-}, \\
\Theta_1 &= e^{-4q_0 \sin(\vartheta_1) (-\frac{1}{2}x - \beta q_0^2 t + i\delta q_0 \cos(\vartheta_1) t - 2\beta q_0^2 \cos(\vartheta_1)^2 t) - i\vartheta_1 + 2i\theta_-}, \\
\Theta_2 &= e^{4q_0 \sin(\vartheta_1) (\frac{1}{2}x + \beta q_0^2 t + i\delta q_0 \cos(\vartheta_1) t + 2\beta q_0^2 \cos(\vartheta_1)^2 t) + i\vartheta_1 + 2i\theta_-}, \\
\Theta_3 &= e^{4q_0 \sin(\vartheta_1) (x + 2\beta q_0^2 t + 4\beta q_0^2 \cos(\vartheta_1)^2 t)}, \\
\Theta_4 &= e^{4q_0 (\sin(\vartheta_1) x + \beta q_0^2 \sin(3\vartheta_1) t + 3\beta q_0^2 \sin(\vartheta_1) t)}.
\end{aligned} \tag{3.30}$$

Through choosing different parameters, the three different dynamic behaviors are presented in Figs. 2-4. Of which, the Fig. 2 displays a dark soliton, Fig. 3 shows a bright-dark soliton, and Fig. 4 exhibits a breather wave. Comparing Fig. 2 and Fig. 3, we find that as the parameters b_1 increase, the dark soliton turns into the bright-dark soliton. On the other hand, from Fig. 3 and Fig. 4, we find that as parameter δ increases and parameter β decreases, the dark soliton changes into the breather wave.

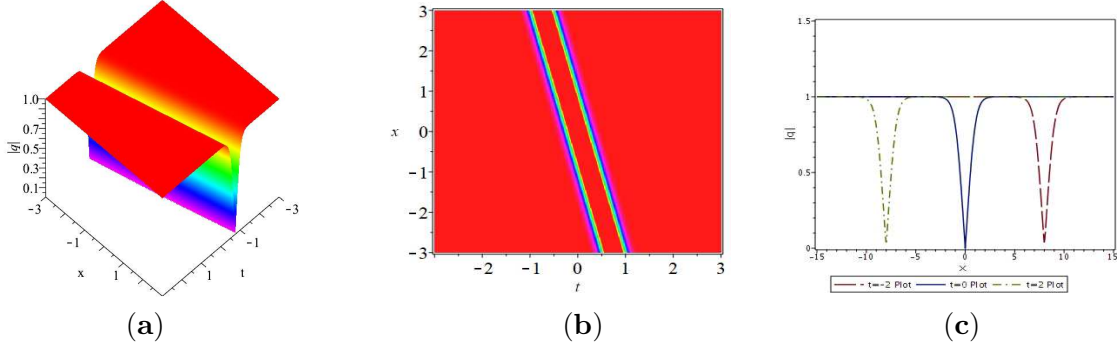


Figure 2. (Color online) Dark soliton solution for Eq.(2.3) with NZBCs. The parameters are $b_1 = 1, q_0 = 1, \vartheta_1 = \frac{\pi}{4}, \theta_- = 0, \delta = \frac{1}{100}, \beta = 1$. (a) Three dimensional plot; (b) The density plot; (c) The wave propagation along the x -axis at $t = -2$ (longdash), $t = 0$ (solid), $t = 2$ (dashdot).

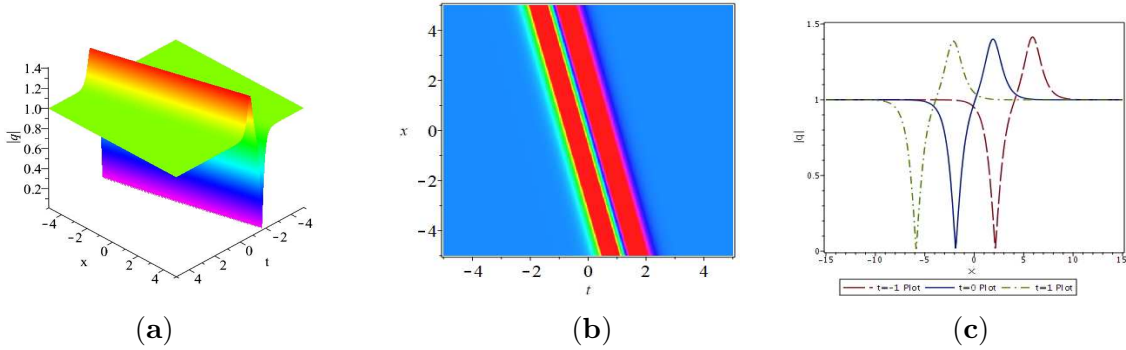


Figure 3. (Color online) Bright-dark soliton solution for Eq.(2.3) with NZBCs. The parameters are $b_1 = 10, q_0 = 1, \vartheta_1 = \frac{\pi}{4}, \theta_- = 0, \delta = \frac{1}{100}, \beta = 1$. (a) Three dimensional plot; (b) The density plot; (c) The wave propagation along the x -axis at $t = -1$ (longdash), $t = 0$ (solid), $t = 1$ (dashdot).

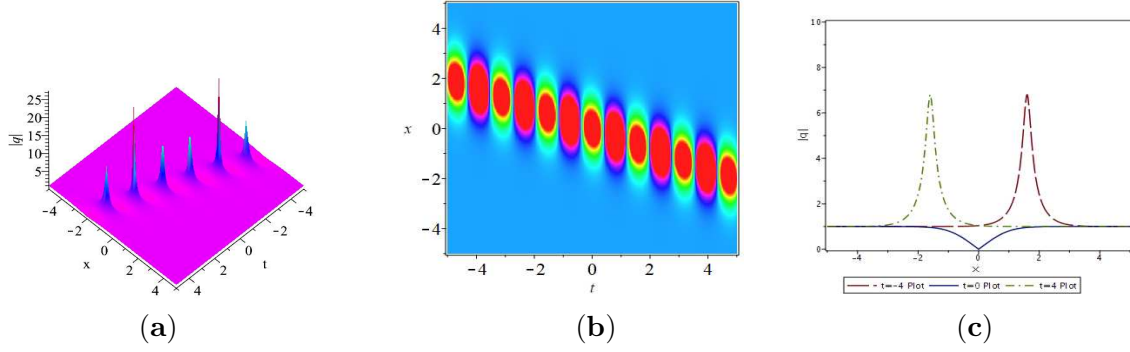


Figure 4. (Color online) Breather solution for Eq.(2.3) with NZBCs. The parameters are $b_1 = 1, q_0 = 1, \vartheta_1 = \frac{\pi}{4}, \theta_- = 0, \delta = 1, \beta = \frac{1}{10}$. (a) Three dimensional plot; (b) The density plot; (c) The wave propagation along the x -axis at $t = -4$ (longdash), $t = 0$ (solid), $t = 4$ (dashdot).

Case 2: $N = 2$

Let $z_1 = q_0 e^{i\vartheta_1}, z_2 = q_0 e^{i\vartheta_2}, \vartheta_1, \vartheta_2 \in (0, \frac{\pi}{2})$. Let $q_- = q_0 e^{i\theta_-}, \theta_- \in \{0, \pi\}, b[\zeta_1] = b_1, b[\zeta_2] = b_2$, where b_1, b_2 are all arbitrary parameter. We obtain the 2-eigenvalue solution, which displays the interaction of two bright-dark soliton solutions(see Fig. 5). As shown in Fig. 5, we can easily see when $t = -8$ (before the interaction), the wave profile consists of two bright-dark solitons, when $t = 0$ (they have the strong interaction), the wave profile creates two spikes. When $t = 8$ (after the interaction), the wave profile restores the original shape.

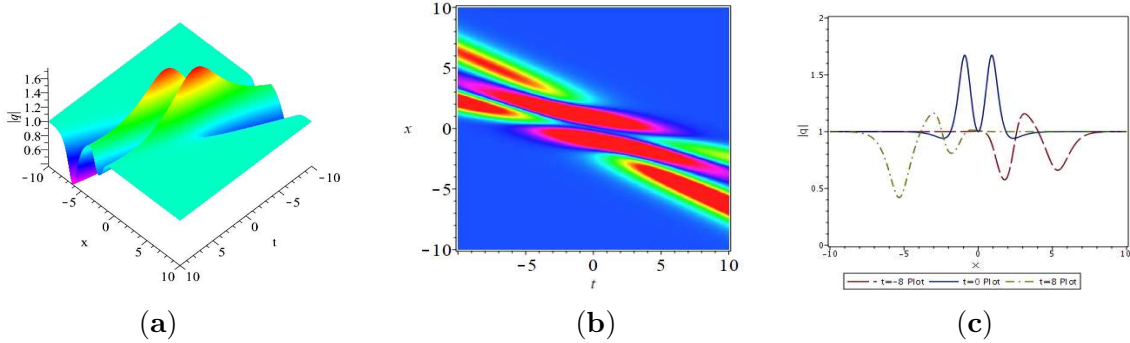


Figure 5. (Color online) The 2-eigenvalue solution for Eq.(2.3) with NZBCs. The parameters are $b_1 = -1, b_2 = -1, q_0 = 1, \vartheta_1 = \frac{\pi}{6}, \vartheta_2 = \frac{\pi}{3}, \theta_- = 0, \delta = \frac{1}{100}, \beta = \frac{1}{10}$. (a) Three dimensional plot; (b) The density plot; (c) The wave propagation along the x -axis at $t = -8$ (longdash), $t = 0$ (solid), $t = 8$ (dashdot).

4 The data-driven soliton solutions for the nonlocal Hirota equation via PINN algorithm

In this section, the PINN algorithm is used to learn the soliton solutions for the nonlocal Hirota equation (2.3) with Dirichlet boundary conditions, given by

$$\begin{cases} q_t + \delta [q_{xx} - 2q^2 q^*(-x, -t) + 2q_0^2 q] + \beta [q_{xxx} - 6qq^*(-x, -t)q_x] = 0, \\ x \in [x_0, x_1], \quad t \in [t_0, t_1], \quad q(x, t_0) = q_0(x), \\ q(x_0, t) = q_{lb}(t), \quad q(x_1, t) = q_{ub}(t), \end{cases} \quad (4.1)$$

where x_0, x_1 denote the corresponding boundaries of x , t_0, t_1 are initial and final times of t . The $q_0(x)$ defines the initial condition. We would apply PINN scheme to investigate the data-driven soliton solutions of Eq.(4.1) with $\delta = 0.01, \beta = 1$. The soliton solutions include the dark soliton solution and bright-dark soliton wave. These solutions have been derived in section 3, and their corresponding dynamic behavior also have been discussed above. As presented in (3.29), the precise form of these solutions can be written as follows:

Using the same parameters as Fig. 2, the exact dark soliton solution admits

$$q(x, t) = \frac{-2\sqrt{2}ie^{\sqrt{2}(4t+x)} \sin(\frac{t}{50}) - e^{2\sqrt{2}(4t+x)} + 1}{2\sqrt{2}ie^{\sqrt{2}(4t+x)} \cos(\frac{t}{50}) - e^{2\sqrt{2}(4t+x)} + 1}. \quad (4.2)$$

Using the same parameters as Fig. 3, the exact bright-dark soliton solution admits

$$q(x, t) = \frac{\sqrt{2}e^{4\sqrt{2}t+\sqrt{2}x-\frac{it}{50}} - 100\sqrt{2}e^{4\sqrt{2}t+\sqrt{2}x+\frac{it}{50}} - 10e^{2\sqrt{2}(4t+x)} + 10}{\sqrt{2}ie^{4\sqrt{2}t+\sqrt{2}x-\frac{it}{50}} + 100\sqrt{2}ie^{4\sqrt{2}t+\sqrt{2}x+\frac{it}{50}} - 10e^{2\sqrt{2}(4t+x)} + 10}. \quad (4.3)$$

4.1 The PINN algorithm

In this subsection, we commit to introduce the PINN algorithm [4] for the data-driven solutions in detail. The main idea of the PINN algorithm is to use a deep neural network to find the solutions of Eq.(4.1). Let $q(x, t) = u(x, t) + iv(x, t)$, $q^*(-x, -t) = u(-x, -t) - iv(-x, -t)$ being its real and imaginary parts, respectively, and then substituting them into Eq.(4.1), we have

$$\begin{cases} u_t + \beta u_{xxx} + \delta u_{xx} - 6\beta[uu(-x, -t) + vv(-x, -t)]u_x - 2\delta u^2 u(-x, -t) \\ -6\beta[uv(-x, -t) - vu(-x, -t)]v_x + 2\delta[1 - 2vv(-x, -t)]u + 2\delta v^2 u(-x, -t) = 0, \\ v_t + \beta v_{xxx} + \delta v_{xx} + 6\beta[uv(-x, -t) - vu(-x, -t)]u_x - 2\delta v^2 v(-x, -t) \\ -6\beta[uu(-x, -t) + vv(-x, -t)]v_x + 2\delta[1 - 2uu(-x, -t)]v + 2\delta u^2 v(-x, -t) = 0. \end{cases} \quad (4.4)$$

Then the physics-informed neural networks $f_u(x, t), f_v(x, t)$ can be defined as

$$\begin{cases} f_u := u_t + \beta u_{xxx} + \delta u_{xx} - 6\beta[uu(-x, -t) + vv(-x, -t)]u_x - 2\delta u^2 u(-x, -t) \\ -6\beta[uv(-x, -t) - vu(-x, -t)]v_x + 2\delta[1 - 2vv(-x, -t)]u + 2\delta v^2 u(-x, -t), \\ f_v := v_t + \beta v_{xxx} + \delta v_{xx} + 6\beta[uv(-x, -t) - vu(-x, -t)]u_x - 2\delta v^2 v(-x, -t) \\ -6\beta[uu(-x, -t) + vv(-x, -t)]v_x + 2\delta[1 - 2uu(-x, -t)]v + 2\delta u^2 v(-x, -t), \end{cases} \quad (4.5)$$

of which $u(x, t; w, b), v(x, t; w, b)$ represent the output of the neural network, which is an approximation of the solution $q(x, t)$. Applying automatic differentiation mechanism in $u(x, t; w, b), v(x, t; w, b)$, the residual PINN $f_u(x, t), f_v(x, t)$ are given [57]. Then, the multi-hidden-layer deep neural network is used to train the network parameters w, b . To updates training parameters, we construct the following Loss functions which can be minimized via using L-BFGS optimization method [58]

$$Loss_{\Theta} = Loss_u + Loss_v + Loss_{f_u} + Loss_{f_v}, \quad (4.6)$$

with

$$\begin{cases} Loss_u = \frac{1}{N_q} \sum_{i=1}^{N_q} |\hat{u}(x_q^i, t_q^i) - u^i|^2, \\ Loss_v = \frac{1}{N_q} \sum_{i=1}^{N_q} |\hat{v}(x_q^i, t_q^i) - v^i|^2, \\ Loss_{f_u} = \frac{1}{N_f} \sum_{l=1}^{N_f} |f_u(x_f^l, t_f^l)|^2, \\ Loss_{f_v} = \frac{1}{N_f} \sum_{l=1}^{N_f} |f_v(x_f^l, t_f^l)|^2, \end{cases} \quad (4.7)$$

where $\{x_q^i, t_q^i, u^i\}_{i=1}^{N_q}$ and $\{x_q^i, t_q^i, v^i\}_{i=1}^{N_q}$ denote the sampling initial and boundary value training data, respectively. $\{x_f^l, t_f^l\}_{l=1}^{N_f}$ denote the sampling collocation points for f_u and f_v . On the one hand, the loss function (4.6) makes the learning solution approximate the exact one, on the other hand, it makes the hidden \hat{u}, \hat{v} satisfy the target nonlinear partial differential equation (4.1). To understand PINN algorithm more intuitively, the flow chart of PINN algorithm for nonlocal Hirota equation is shown in Fig. 6, in which neural network and physical information part can be seen. The aim is to optimize the loss function using the neural network part as well as the physics information part.

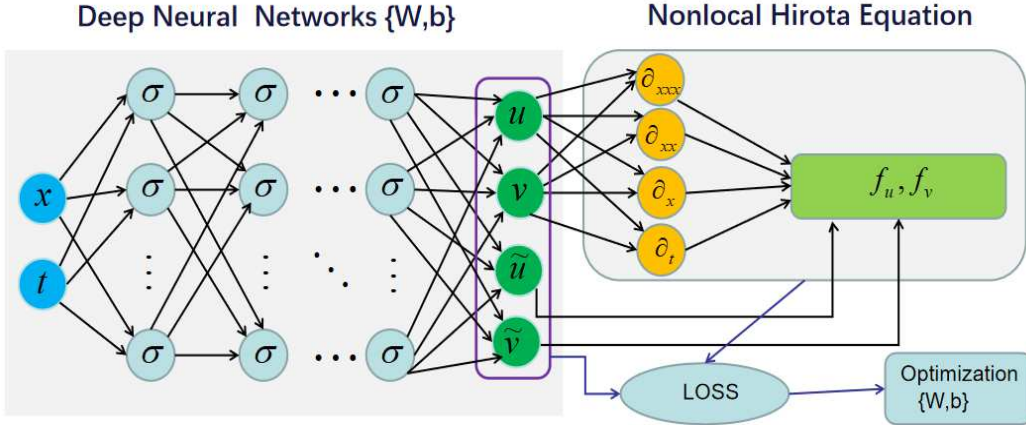


Figure 6. (Color online) The PINN scheme solving the nonlocal Hirota equation, $\tilde{u} = u(-x, -t), \tilde{v} = v(-x, -t)$.

To obtain the data-driven soliton solution for the nonlocal Hirota equation (4.1), we choose the PINN which contains 9-hidden-layer neural network with each layer having 40 neurons. Their activation functions both are the hyperbolic tangent (\tanh). The all codes are written by Python 3.7 and run on Tensorflow 1.15, and the corresponding hardware is a HP Laptop 14s-dr2xxx with 2.40 GHz 4-core 11th Gen Intel Core i5-1135G7 and 16 GB memory.

4.2 The data-driven dark soliton solution

First, we take $[x_0, x_1] = [-3, 3]$ and $[t_0, t_1] = [-3, 3]$ in Eq.(4.1) as the boundary conditions, and select the following initial condition arising from the dark soliton solution (4.2)

$$q_0(x) = q(x, -3), \quad r_0(x) = r(x, -3), \quad (4.8)$$

and the Dirichlet boundary conditions for Eq.(1.2)

$$q_{lb}(t) = q(-3, t), \quad q_{ub}(t) = q(3, t), \quad r_{lb}(t) = r(-3, t), \quad r_{ub}(t) = r(3, t), \quad t \in [-3, 3]. \quad (4.9)$$

In terms of MATLAB software, the traditional finite difference method can be used to capture the original training data by dispersing Eq.(4.2) with dividing spatial region $[-3, 3]$ into 1500 points and time region $[-3, 3]$ into 1000 points. The original training data contains the initial boundary data and the inner points. Here, we choose $N_q = 1500$ as the random sample points from initial boundary data and $N_f = 30000$ as random collocation points from the inner points based on the Latin hypercube sampling (LHS) method [59]. Processing these obtained training data in the PINN scheme, the data-driven dark soliton solution $q(x, t)$ can be eventually learned, which has a $2.695814\text{e-}04$ \mathbb{L}_2 -norm error compared with the exact one. The total learning process executes 927 times and takes about 1262.4172 seconds. The corresponding dynamic behaviors are displayed in following Figs. 7 and 8.

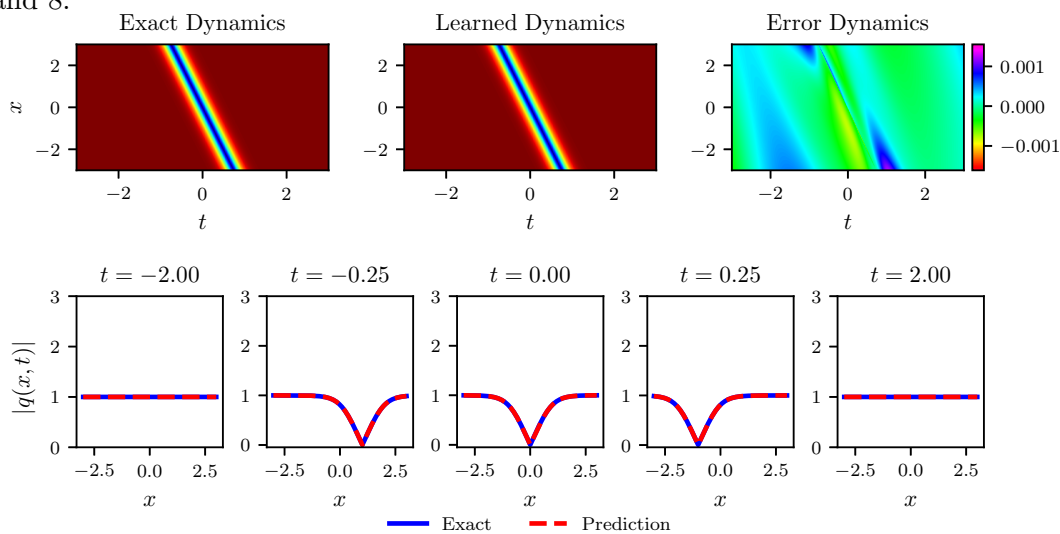


Figure 7. (Color online) The data-driven dark soliton solution $q(x, t)$ for nonlocal Hirota equation (4.1): The exact, learned and error dynamics density plots, and the sectional drawings which contain the learned and explicit dark soliton solution $q(x, t)$ at the five distinct times $t = -2, t = -0.25, t = 0, t = 0.25, t = 2$.

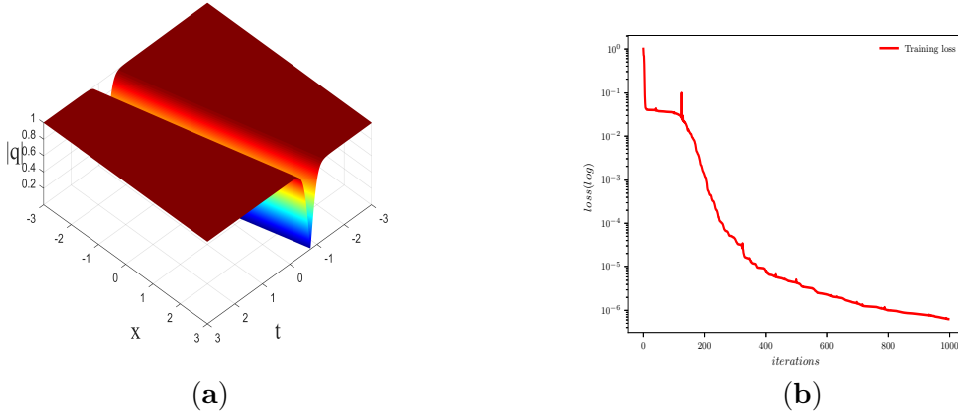


Figure 8. (Color online) The data-driven dark soliton solution $q(x, t)$ for nonlocal Hirota equation (4.1): (a) The three-dimensional plot; (b) The loss curve figure.

In Fig. 7, the wave propagation pattern along the x -axis and the density plots for the data-driven dark soliton solution are shown respectively. From the Fig.7, it is easy to find that the error range is about -0.001 to 0.001 between the learned dynamics and error dynamics. This fact can verify the simulation is pretty good. The Fig. 8 is the three-dimensional plot and loss curve figure of data-driven dark soliton solution.

4.3 The data-driven bright-dark soliton solution

For data-driven periodic wave solution, we let $[x_0, x_1] = [-5, 5]$ and $[t_0, t_1] = [-5, 5]$ in Eq.(4.1) as the boundary conditions, and select the following initial condition arising from the bright-dark wave solution(4.3)

$$q_0(x) = q(x, -5), \quad r_0(x) = r(x, -5), \quad (4.10)$$

and the Dirichlet boundary conditions

$$q_{lb}(t) = q(-5, t), \quad q_{ub}(t) = q(5, t), \quad r_{lb}(t) = r(-5, t), \quad r_{ub}(t) = r(5, t), \quad t \in [-5, 5]. \quad (4.11)$$

Carrying out the same process as subsection 4.2, the data-driven bright-dark soliton solution is generated successfully. The results of the experiment show that the L_2 -norm error between learning solution $q(x, t)$ and exact one is $8.243617e-04$, and the whole learning process iterates 1807 times with costing 2737.0690 seconds. The main dynamic behaviors for the data-driven bright-dark soliton solution are plotted in Figs.9 and 10. From these plots, we also find the learning effect is pretty good with a very small error and a rapidly decaying Loss curve.

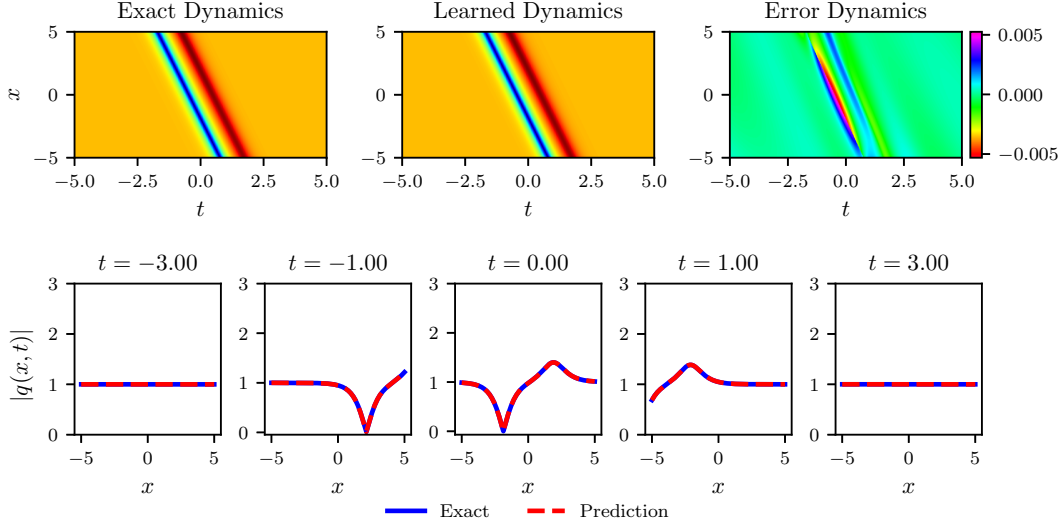


Figure 9. (Color online) The data-driven bright-dark soliton solution $q(x, t)$ for nonlocal Hirota equation (4.1): The exact, learned and error dynamics density plots, and the sectional drawings which contain the learned and explicit bright-dark soliton solution $q(x, t)$ at the five distinct times $t = -3, t = -1, t = 0, t = 1, t = 3$.

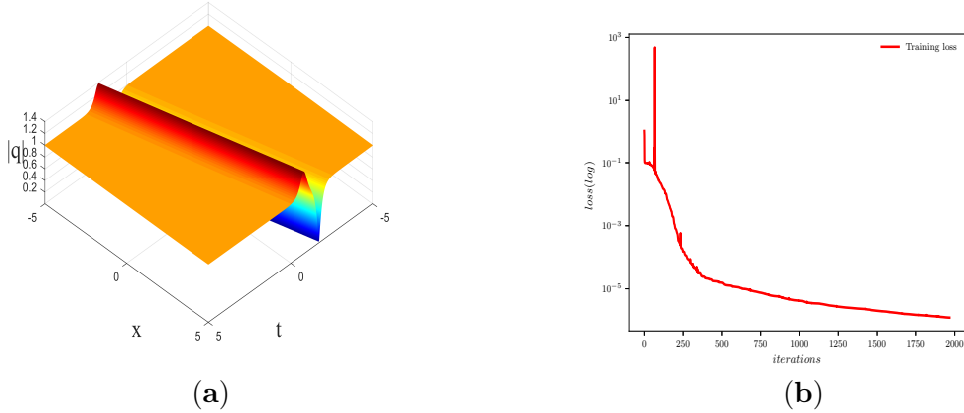


Figure 10. (Color online) The data-driven bright-dark soliton solution $q(x, t)$ for nonlocal Hirota equation (4.1): (a) The three-dimensional plot; (b) The loss curve figure.

4.4 The PINN algorithm for the data-driven parameter discovery

In this section, we put our attention to the problem of data-driven discovery of nonlocal Hirota equation (4.1) by using PINN algorithm. Our goal is to identify the parameters δ, β in terms of the dark soliton solution (4.2). In the same way, the physics-informed neural networks $f_u(x, t), f_v(x, t)$ for the equation (4.1) are given in (4.5).

Using the Latin Hypercube Sampling, a training data set can be generated through selecting randomly $N_q = 1500$ as the initial boundary data and $N_f = 30000$ as the collocation points with the aid of the exact soliton solution (4.2) with $\delta = 0.01, \beta = 1$ and

$(x, t) \in [-3, 3] \times [-3, 3]$. In terms of the obtained training data set, using a 9-hidden-layer deep PINN with 40 neurons per layer, the data-driven parameters δ, β can be discovered. The corresponding results are summarized in Table 1. We observe that the PINN is able to correctly identify the unknown parameters with very high accuracy when the training data was corrupted without noise. Specifically, as we can see in Table 1, at the case of 0.005 noise and 0.01 noise, the error of parameters δ and β is still receivable, which illustrates that the predictions remain robust. Of course, we can also find that noise has a bad effect on the error value of parameters.

Table 1: Data-driven parameter discovery of δ, β in the sense of dark soliton

Parameter \ Noise	δ	error of δ	β	error of β
Correct parameter	0.01	0	1	0
Without noise	0.00976523	2.34770×10^{-2}	0.9998441	1.559×10^{-4}
With a 0.005 noise	0.01055261	5.52606×10^{-2}	0.9998072	1.928×10^{-4}
With a 0.01 noise	0.00934824	6.51762×10^{-2}	0.9998599	1.401×10^{-4}

The variation of unknown parameters and loss functions with iteration is analyzed when different noises are used in inverse problems. Figs. 11(a) and (b) show the changes of unknown parameters with iteration under different noises. We find that the unknown parameters fluctuate less in the absence of noise, but the parameters fluctuate more as the noise increases. Fig. 11(c) depicts the changes of loss functions for different noises as the number of iterations increases. It indicates that the convergence effect becomes worse and worse with the increase of noise. Therefore, we can conclude that when discovering the physical parameters of the model, the less noise the better the training effect.

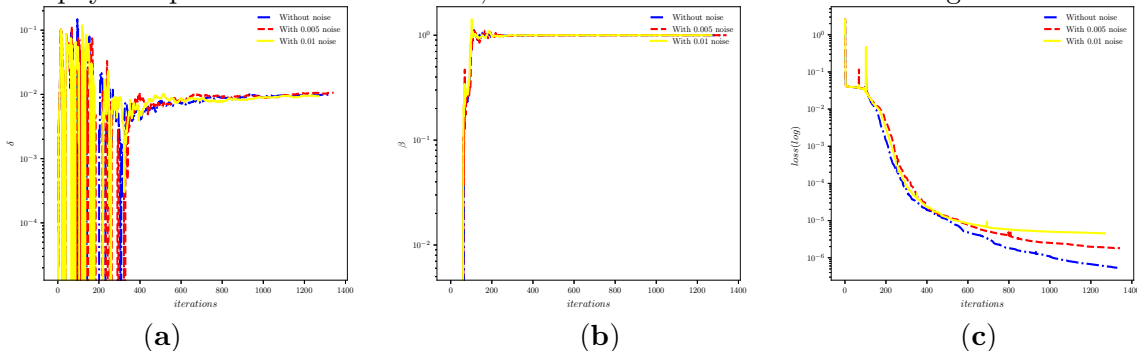


Figure 11. (Color online)(a, b) the variation of unknown parameters δ, β and (c) the variation of loss function with the different noise.

5 Conclusion

In this paper, we have applied the RH method to discuss the nonlocal Hirota equation with NZBCs. Through solving the RH problem at the case of simplify poles, we have given out the general N -soliton solutions for the nonlocal Hirota equation under NZBCs. The critical technique shown in this work is to eliminate the properties of singularities via subtracting

the residue from the original non-regular RH problem when reflection coefficients have simplify poles. Additionally, the asymptotic value of jump matrix is subtracted from the original non-regular RH problem. Then the regular RH problem can be displayed, which can be solved by Plemelj formula. Finally, the simplify poles N -soliton solutions can be derived by using the solution of RH problem to reconstruct potential function. Compared with the local Hirota equation, the Symmetry reductions of Just solutions and scattering matrix is different, which results in a disparate discrete spectra distribution. The dynamical patterns of one-soliton and two-soliton have been discussed in detail. For one-soliton, the dark soliton, bright-dark soliton, breather wave were displayed respectively by selecting different parameters. For two-soliton, elastic collision and interactions between the two one-soliton solution from weak to strong have been analyzed at length.

Additionally, we have also studied the data-driven soliton solutions and parameters discovery for the nonlocal Hirota equation with Dirichlet boundary conditions via the PINN method. Remarkably, due to the nonlocal Hirota equation has \mathcal{PT} symmetry term, it is quite different with the local Hirota equation. Through adding the nonlocal term into the NN, we can successfully handle the \mathcal{PT} symmetry term and give out the data-driven soliton solutions and the parameter prediction for the nonlocal Hirota equation. Our results indicate that the deep learning can be applied to solve nonlocal integrable systems.

Acknowledgements

This work was supported by the project is supported by National Natural Science Foundation of China(No.12175069) and Science and Technology Commission of Shanghai Municipality (No.21JC1402500 and No.18dz2271000).

References

- [1] R. Hirota, Direct Methods in Soliton Theory, Springer, Berlin, 2004.
- [2] V. B. Matveev, M. A. Salle, Darboux Transformation and Solitons, Springer, Berlin, 1991.
- [3] M. J. Ablowitz, P. A. Clarkson, Solitons; Nonlinear Evolution Equations and Inverse Scattering, Cambridge University Press, Cambridge, 1991.
- [4] M. Raissi, P. Perdikaris, G. E. Karniadakis, Physics-informed neural networks: A deep learning framework for solving forward and inverse problems involving nonlinear partial differential equations. *J. Comput. Phys.* 378, 686-707 (2019).
- [5] C. S. Gardner, J. M. Greene, M. D. Kruskal, R. M. Miura, Method for solving the KortewegdeVries equation. *Phys. Rev. Lett.* 19, 1095-7(1967).
- [6] V. E. Zakharov, S. V. Manakov, S. P. Novikov, L. P. Pitaevskii, The Theory of Solitons: The Inverse Scattering Method, Consultants Bureau, New York, (1984).

- [7] J. Yang, *Nonlinear Waves in Integrable and Non-integrable Systems*, Society for Industrial and Applied Mathematics (2010).
- [8] Y. Li, S. F. Tian, J. J. Yang, Riemann-Hilbert problem and interactions of solitons in the n -component nonlinear Schrödinger equations. *Stud. Appl. Math.*, (2021).
- [9] B. L. Guo, L. M. Ling, Riemann-Hilbert approach and N -soliton formula for coupled derivative Schrödinger equation, *J. Math. Phys.* 53, 133-3966(2012).
- [10] W. Q. Peng, S. F. Tian, X. B. Wang, et al. Riemann-Hilbert method and multi-soliton solutions for three-component coupled nonlinear Schrödinger equations. *J. Geom. Phys.*, 146, 103508(2019).
- [11] B. Yang, Y. Chen, High-order soliton matrices for Sasa-Satsuma equation via local Riemann-Hilbert problem. *Nonlinear Anal. Real World Appl.*, 45, 918-941(2019).
- [12] X. G. Geng, J. P. Wu, Riemann-Hilbert approach and N -soliton solutions for a generalized Sasa-Satsuma equation. *Wave Motion.* 60, 62-72 (2016).
- [13] Y. S. Zhang, J. G. Rao, Y. Cheng, J. S. He, Riemann-Hilbert method for the Wadati-Konno-Ichikawa equation N simple poles and one higher-order pole. *Physica D* 399, 173-185 (2019).
- [14] D. S. Wang, D. J. Zhang, J. Yang, Integrable properties of the general coupled nonlinear Schrödinger equations. *J. Math. Phys.* 51, 023510 (2010).
- [15] G. Biondini, G. Kovačič, Inverse scattering transform for the focusing nonlinear Schrödinger equation with nonzero boundary conditions, *J. Math. Phys.* 55, 031506 (2014).
- [16] G. Biondini, E. Fagerstrom, B. Prinari, Inverse scattering transform for the defocusing nonlinear Schrödinger equation with fully asymmetric non-zero boundary conditions, *Physica D*, 333, 117-136 (2016).
- [17] G. Q. Zhang, Z. Y. Yan, Inverse scattering transforms and soliton solutions of focusing and defocusing nonlocal mKdV equations with non-zero boundary conditions. *Physica D.* 402, 132170 (2019).
- [18] N. Liu, B. Guo, Solitons and rogue waves of the quartic nonlinear Schrödinger equation by Riemann-Hilbert approach. *Nonlinear. Dyn.* 100, 629-646 (2020).
- [19] Z. C. Zhang, E. G. Fan, Inverse scattering transform for the Gerdjikov-Ivanov equation with nonzero boundary conditions. *Z. Angew. Math. Phys.*, 71(2020).
- [20] D. Bilman, P. D. Miller, A Robust inverse scattering transform for the focusing nonlinear Schrödinger equation. *Comm Pure Appl Math.* 72(8), 1722-1805(2019).
- [21] S. Y. Chen, Z. Y. Yan, The higher-order nonlinear Schrödinger equation with non-zero boundary conditions: robust inverse scattering transform, breathers, and rogons. *Phys Lett A.*, 383(29), 125906(2019).

- [22] X. E. Zhang, Y. Chen, Inverse scattering transformation for generalized nonlinear Schrödinger equation. *Appl. Math. Lett.* 98, 306-313(2019).
- [23] J. Li, Y. Chen, Solving second-order nonlinear evolution partial differential equations using deep learning, *Commun. Theor. Phys.* 72, 105005(2020).
- [24] J. C. Pu, J. Li, Y. Chen. Soliton, Breather and Rogue Wave Solutions for Solving the Nonlinear Schrödinger Equation Using a Deep Learning Method with Physical Constraints. *Chin. Phys. B* (2021).
- [25] J. C. Pu, J. Li, Y. Chen, Solving localized wave solutions of the derivative nonlinear Schrödinger equation using an improved PINN method. *Nonlinear Dyn.*, 105(2), 1-17(2021).
- [26] W. Q. Peng, J. C. Pu, Y. Chen, PINN deep learning for the Chen-Lee-Liu equation: rogue wave on the periodic background. *Commun. Nonlinear Sci. and Numer. Simul.* 105, 106067 (2022).
- [27] Z. W. Miao, Y. Chen, physics-informed neural network method in high-dimensional integrable systems, arXiv: 2107.02985, 2021.
- [28] J. C. Pu, Y. Chen, The data-driven vector localized waves of Manakov system using improved PINN approach. arXiv preprint arXiv:2109.09266, 2021.
- [29] S. N. Lin, Y. Chen, A two-stage physics-informed neural network method based on conserved quantities and applications in localized wave solutions, arXiv: 2107.01009, 2021.
- [30] L. Wang, Z. Y. Yan. Data-driven rogue waves and parameter discovery in the defocusing nonlinear Schrödinger equation with a potential using the PINN deep learning. *Phys. Lett. A*, 127408 (2021).
- [31] Y. Fang, G. Z. Wu, Y. Y. Wang, C. Q. Dai, Data-driven femtosecond optical soliton excitations and parameters discovery of the high-order NLSE using the PINN. *Nonlinear Dyn.*, 1-14 (2021).
- [32] G. Z. Wu, Y. Fang, Y. Y. Wang, G. C. Wu, C. Q. Dai, Predicting the dynamic process and model parameters of the vector optical solitons in birefringent fibers via the modified PINN. *Chaos, Soliton Fract.*, 152, 111393(2021).
- [33] Y. F. Mo, L. M. Ling, D. L. Zeng, Data-driven vector soliton solutions of coupled nonlinear Schrödinger equation using a deep learning algorithm. *Phys. Lett. A*, 127739 (2021).
- [34] R. El-Ganainy, K. Makris, D. Christodoulides, Z. H. Musslimani, Theory of coupled optical \mathcal{PT} -symmetric structures. *Opt Lett.* 32, 2632 (2007).
- [35] C. M. Bender, B. K. Berntson, D. Parker, E. Parker, Observation of PT phase transition in a simple mechanical system. *Am J Phys.* 81, 173 (2013).

- [36] T. Gadzhimuradov, A. Agalarov, Towards a gauge-equivalent magnetic structure of the nonlocal nonlinear Schrödinger equation. *Phys Rev A*. 93, 62124 (2016).
- [37] C. M. Bender, S. Boettcher, H. F. Jones, P. N. Meisinger, M. Simsek, Bound states of non-Hermitian quantum field theories. *Phys Lett A*. 71, 1095(2003).
- [38] B. Bagchi, C. Quesne, $Sl(2, C)$ as a complex Lie algebra and the associated non-Hermitian Hamiltonians with real eigenvalues. *Phys Lett A*. 273, 285(2000).
- [39] D. Mihalache, Multidimensional localized structures in optical and matter-wave media: a topical survey of recent literature. *Rom Rep Phys*. 69, 403(2017).
- [40] M. J. Ablowitz, Z. H. Musslimani, Integrable nonlocal nonlinear Schrödinger equation. *Phys Rev Lett*. 110, 64105 (2013).
- [41] A. S. Fokas, Integrable multidimensional versions of the nonlocal nonlinear Schrödinger equation. *Nonlinearity*. 29, 319 (2016).
- [42] J. G. Rao, Y. Cheng, and J. S. He, Rational and semi-rational solutions of the nonlocal Davey-Stewartson equations, *Stud. Appl. Math*. 139, 568 (2017).
- [43] Z. X. Zhou, Darboux transformations and global explicit solutions for nonlocal Davey-Stewartson I equation, *Stud. Appl. Math*. 141, 186 (2018).
- [44] M. M. Wang, Y. Chen, Dynamic behaviors of general N -solitons for the nonlocal generalized nonlinear Schrödinger equation. *Nonlinear Dyn.*, 104, 2621-2638 (2021).
- [45] H. J. Zhou, Y. Chen, Breathers and rogue waves on the double-periodic background for the reverse-space-time derivative nonlinear Schrödinger equation. *Nonlinear Dyn.* (2021).
- [46] M. J. Ablowitz and Z. H. Musslimani, Inverse scattering transform for the integrable nonlocal nonlinear Schrödinger equation, *Nonlinearity* 29, 915-946 (2016).
- [47] M. J. Ablowitz and Z. H. Musslimani, Integrable nonlocal nonlinear equations, *Stud. Appl. Math*. 139, 7-59(2017).
- [48] J. L. Ji and Z. N. Zhu, Soliton solutions of an integrable nonlocal modified Korteweg-de Vries equation through inverse scattering transform, *J. Math. Anal. Appl*. 453, 973-984(2017).
- [49] M. J. Ablowitz, X. D. Luo, and Z. H. Musslimani, Inverse scattering transform for the nonlocal nonlinear Schrödinger equation with nonzero boundary conditions, *J. Math. Phys*. 59, 011501(2018).
- [50] M. J. Ablowitz, B. F. Feng, X. D. Luo, and Z. H. Musslimani, Reverse space-time nonlocal sine-gordon/sinh-gordon equations with nonzero boundary conditions, *Stud. Appl. Math*. 141, 267-307(2018).
- [51] G. Q. Zhang, Z. Y. Yan, Inverse scattering transforms and soliton solutions of focusing and defocusing nonlocal mKdV equations with nonzero boundary conditions. *Physica D*, 402, 132170(2020).

- [52] X. F. Zhang, S. F. Tian, J. J. Yang, Inverse scattering transform and multiple high-order pole solutions for the nonlocal focusing and defocusing modified Korteweg-de Vries equation with the nonzero boundary conditions. arXiv preprint arXiv:2109.02901, 2021.
- [53] J. Cen, C. Francisco, F. Andreas, Integrable nonlocal Hirota equations. *J Math. Phys.* 60(8), 081508 (2019).
- [54] Y. Li, S. F. Tian, Inverse scattering transform and soliton solutions of an integrable nonlocal Hirota equation. *Commun. Pur. Appl. Anal.*, (2021).
- [55] Y. R. Xia, R. X. Yao, X. P. Xin, Darboux transformation and soliton solutions of a nonlocal Hirota equation. *Chinese Physics B* (2021).
- [56] N. N. Li, R. Guo, Nonlocal continuous Hirota equation: Darboux transformation and symmetry broken and unbroken soliton solutions, *Nonlinear Dyn*, 105, 617-628 (2021).
- [57] A. G. Baydin, B. A. Pearlmutter, A. A. Radul, J. M. Siskind, Automatic differentiation in machine learning: a survey, *J. Mach. Learning Research*, 18, 1-43(2018).
- [58] D. C. Liu, J. Nocedal, On the limited memory BFGS method for large scale optimization, *Math. Program* 45, 503-528(1989).
- [59] M. Stein, Large sample properties of simulations using Latin hypercube sampling. *Technometrics*, 29, 143-151 (1987).